ACS APPLIED MATERIALS & INTERFACES

Research Article

www.acsami.org

Sub-10 nm Sr_2LuF_7:Yb/Er@Sr_2GdF_7@SrF_2 Up-Conversion Nanocrystals for Up-Conversion Luminescence–Magnetic Resonance–Computed Tomography Trimodal Bioimaging

Cailing Chen,[†] Jianhua Liu,[†,‡] Ying Chen,[§] Chunguang Li,[*,†] Xiaomin Liu,[//] He Huang,[†] Chen Liang,[†] Yue Lou,[†] Zhan Shi,[*,†] and Shouhua Feng[†]

[†]State Key Laboratory of Inorganic Synthesis and Preparative Chemistry, College of Chemistry, Jilin University, Changchun 130012, P.R. China

[‡]Department of Radiology, The Second Hospital of Jilin University, Changchun 130022, P.R. China

[§]Department of Obstetrics, First Hospital of Jilin University, 71 Xinmin Street, Changchun 130021, China

[//]State Key Laboratory of Luminescence and Applications, Changchun Institute of Optics, Fine Mechanics and Physics, Chinese Academy of Sciences, Changchun 130012, P.R. China

Supporting Information

ABSTRACT: Herein, sub-10 nm core–shell nanocrystals (NCs), which select Sr_2LuF_7:Yb/Er as core, Sr_2GdF_7 as middle shell, and SrF_2 as an outermost shell, were synthesized by a seed-mediated growth process. The NCs possess good crystallinity, morphology, and up-conversion luminescent properties. After modification by polyethylenimine branched (PEI), in vitro cell up-conversion imaging with low autofluorescence was realized. Due to the presence of Gd^{3+} ions, in vivo magnetic resonance (MR) imaging was also achieved with these designed NCs. More significantly, these special core–shell NCs exhibited high contrast in in vivo X-ray computed tomography (CT) imaging because of their good X-ray absorption ability. These results indicate that the core–shell up-conversion NCs can serve as promising contrast agents for up-conversion luminescence–MR–CT trimodal bioimaging.

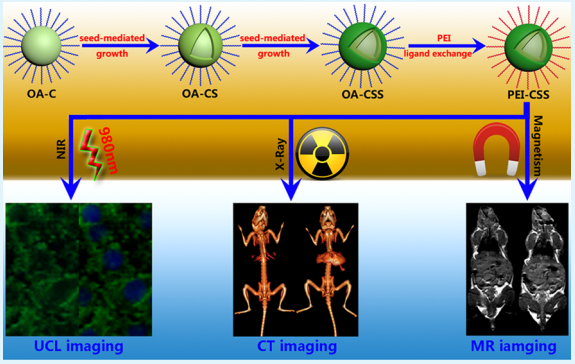

KEYWORDS: *rare earth, core–shell, nanocrystal, up-conversion, muti-modal bioimaging*

1. INTRODUCTION

In recent years, biological imaging technologies have aroused great interest for the detection and treatment of diseases due to their visualization capabilities and noninvading nature to organisms.[1−5] There are many bioimaging methods with specific uses in clinical medicine. Fluorescent imaging has high sensitivity and high spatial and temporal resolution.[6−8] Computed X-ray tomography (CT) imaging has high sensitivity for tissues such as bone, and magnetic resonance (MR) imaging is safe and confers certain advantages for soft tissues over CT.[2,9−11] However, in many cases, single-mode bioimaging cannot meet to diagnose those difficult miscellaneous diseases. Therefore, multimodal bioimaging sets off a frenzy in biomedical areas.[1,12,13] Multimodal probes combining two or more functions together can improve the sensitivity for biomedical detection and treatment.[1,14−16] Lanthanide-doped up-conversion nanomaterial as a kind of bioimaging agent, without autofluorescence, has been widely used in biomedical detection and treatment by many groups.[17−19] However, the bottleneck of up-conversion nanomaterials is low quantum yield compared with traditional luminescence materials, such as semiconductor quantum dots (QDs) and organic fluorescent dyes, which limits its application in various fields.[20,21] To improve the quantum yield, materials researchers have reported a number of strategies, such as plasmon resonance enhancement,[22,23] local crystal field adjustment,[24,25] and core–shell structure.[26,27] Among these strategies, core–shell structure can reduce surface-related quenching and suppress cross-relaxation to enhance luminescence efficiency.[28] Another merit of core–shell structure is that it can introduce other optical, electrical, and magnetic properties.[29,30] The nanostructure with small size is conducive to bioapplication, but the synthesis of sub-10 nm core–shell up-conversion nanoparticles remains a considerable challenge because the increase of shell thickness will lead to the increase of size.[31−33] At present, there are many reports about $AREF_4$ (A = alkaline metal, RE = rare earth),[33−37] but B_2REF_7 (B = alkaline earth) as an important kind of fluoride matrix has rarely been reported. Some efforts have been made to study

Received: November 2, 2016
Accepted: January 19, 2017
Published: February 7, 2017

DOI: 10.1021/acsami.6b14007
ACS Appl. Mater. Interfaces 2017, 9, 5748−5756

Scheme 1. Schematic Illustration of the Preparation of PEI-Capped SLF@SGF@SF and Its Bioapplication

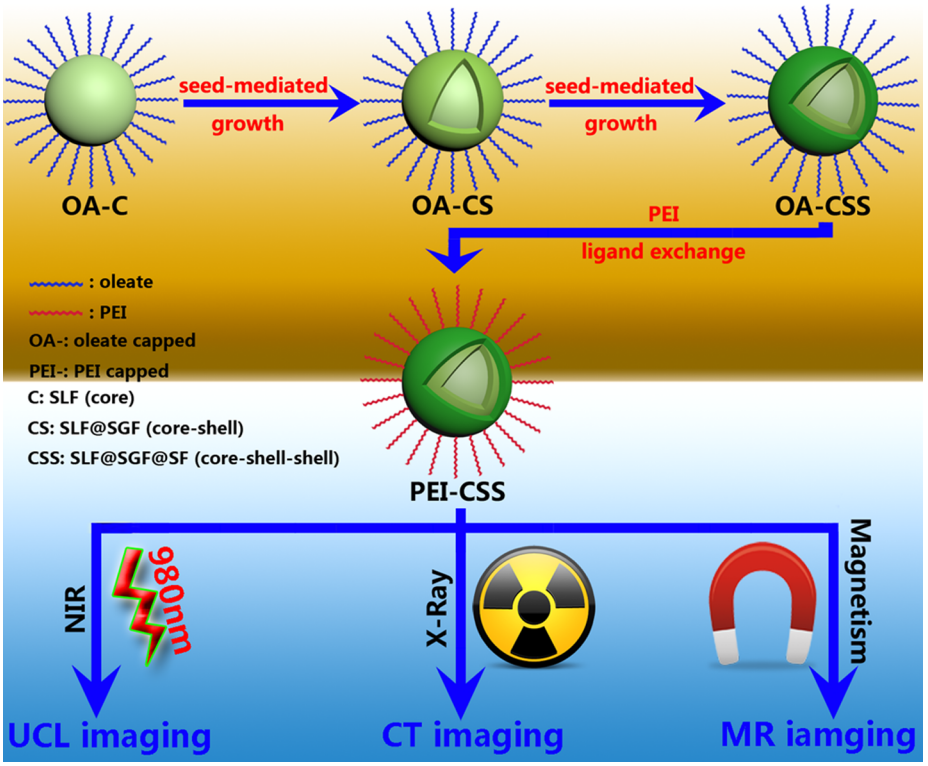

B_2REF_7. For example, Chen's group reported the synthesis, optical properties and application of Sr_2YF_7 nanocrystals (NCs)[38] and the hydro(solvo)thermal synthesizes of Sr_2LuF_7 and Sr_2GdF_7 has also been reported.[39] However, to date, systematic reports about the properties and application of Sr_2LnF_7 (Ln = Gd or Lu) are still lacking.

In this article, we carefully designed and synthesized sub-10 nm Sr_2LuF_7:Yb/Er@Sr_2GdF_7@SrF_2 (SLF@SGF@SF) core–shell up-conversion NCs via a seed-mediated growth process. Each part of this design has its own unique role and works together to achieve trimodal imaging. Needless to say, two inert shells reduced the surface defects and markedly increased the up-conversion luminescence intensity. The SrF_2 shell can also increase the biological compatibility of NCs because strontium is required by all living systems.[40−42] The methyl thiazolyl tetrazolium (MTT) assay demonstrated the as-prepared core–shell NCs with low biotoxicity. The in vitro cell imaging was realized with the designed core–shell NCs. Due to the magnetism of Gd^{3+} ions in the middle shell, the core–shell nanostructure can also act as contrast agent for in vivo MR imaging. More significantly, this designed core–shell up-conversion nanostructure exhibited high contrast in in vivo CT imaging because of the good X-ray absorption ability of Lu^{3+}, Gd^{3+}, and doped Yb^{3+} and Er^{3+} ions. Preparation of SLF@SGF@SF and their bioapplication is schematically illustrated in Scheme 1.

2. MATERIALS AND METHODS

2.1. Reagents. Polyethylenimine branched [PEI, $M_w \approx 25000$] was achieved from Sigma-Aldrich, Ltd. High-purity (99.99%) Gd_2O_3, Lu_2O_3, Yb_2O_3, Er_2O_3, trifluoroacetate acid (TFA; 99%), 1-octadecene (ODE; 90%), and oleylamine (OAE; C18:90%) were obtained from Energy Chemical, Co., Ltd. $SrCO_3$, ethanol (AR), cyclohexane (AR), diethylene glycol (DEG; CP), and chloroform (AR) were purchased from Sinopharm Chemical Reagent Co. Ltd. Unless otherwise noted, all of the starting chemicals were used as received without further purification.

2.2. Characterization. Powder X-ray diffraction (XRD) was performed on a Rigaku D/Max 2500 diffractometer with $Cu_{K\alpha}$ radiation operating at 200 mA and 40 kV. Transmission electron microscopy (TEM) images were performed using a FEI Tecnai G2 S-Twin with a field emission gun operating at 200 kV. Energy dispersive X-ray (EDX) spectra were collected by means of a JEOL JSM-6300 at 5 kV. The emission spectra of the samples were recorded on an Edinburgh Instruments FLS920 spectrofluorimeter equipped with a 980 nm laser diode as the excitation source. The magnetic properties of the samples were evaluated by an MPMS-XL superconducting quantum interference device magnetometer. The relaxation times of Gd^{3+} with different concentrations were performed on a MesoMR analyzing instrument (Shanghai Niumag Corporation). Images were acquired digitally using a Canon 600D camera with the EF-s 15−135 mm lens.

2.3. Synthesis of NCs. *2.3.1. Preparation of Ln(TFA)$_3$ (Ln = Gd, Lu, Yb and Er) and Sr(TFA)$_2$ Precursors.* Typical procedure: 4 mmol Ln_2O_3 was added into a mixture of 10 mL of TFA and 10 mL of deionized (DI) water. Next, the reaction solution was heated to 100 °C and kept at this temperature for 10 h under continuous stirring until an optically transparent solution formed. The product was filtered to remove any unreacted insolubles and dried in an oven at 100 °C. The $Sr(TFA)_2$ powder was obtained by a similar procedure except that Ln_2O_3 was replaced by $SrCO_3$.

2.3.2. Synthesis of Sr_2LuF_7:Yb,Er (SLF) Core NCs. The SLF-core NCs were prepared with a thermal decomposition method at a high temperature. In a typical procedure, $Lu(TFA)_3$ (0.4 mmol), $Er(TFA)_3$ (0.01 mmol), $Yb(TFA)_3$ (0.09 mmol), and $Sr(TFA)_2$ (1 mmol) were added in a three-necked round-bottom flask (50 mL) containing 10 mL of ODE, 5 mL of OA, and 2 mL of OAE at room temperature. The mixture was exposed to ultrasound until it formed an optically transparent solution. Subsequently, the three-necked round-bottom flask was connected to a Schlenk line and heated to 100 °C under vacuum for 0.5 h. Next, the reaction solution was heated to 300 °C under N_2 gas and the reaction kept at this temperature for 0.5 h. The solution was cooled to room temperature (RT) naturally, and the

DOI: 10.1021/acsami.6b14007
ACS Appl. Mater. Interfaces 2017, 9, 5748−5756

products were precipitated with ethanol, centrifuged, and washed with cyclohexane and ethanol in sequence. Finally, products were redispersed in cyclohexane.

2.3.3. Synthesis of Sr_2LuF_7:Yb,Er@ Sr_2GdF_7 (SLF@SGF) Core–Shell NCs. The SLF core NCs as seeds for the synthesis of SLF@SGF core–shell NCs were obtained as described earlier. First, to obtain shell precursors, $Gd(TFA)_3$ (0.5 mmol), $Sr(TFA)_2$ (1 mmol) 5 mL of ODE, 2.5 mL of OA, and 1 mL of OAE were mixed together in a three-necked round-bottom flask (50 mL) and then heated to 100 °C for 0.5 h. Seeds obtained were mixed with 5 mL of ODE, 2.5 mL of OA, and 1 mL of OAE in a three-necked round-bottom flask (50 mL) and heated to 100 °C for 0.5 h. Subsequently, shell precursors were added, and the solution was connected to a Schlenk line and heated to 100 °C under vacuum for another 0.5 h. Next, the reaction solution was heated to 300 °C for 0.5 h under N_2 gas before cooling to RT naturally. The products were precipitated with ethanol, centrifuged, and washed with cyclohexane and ethanol in sequence. Finally, products were redispersed in cyclohexane.

2.3.4. Synthesis of Sr_2LuF_7:Yb,Er@ Sr_2GdF_7@SrF_2 (SLF@SGF@SF) Core–Shell NCs. The SLF@SGF core–shell NCs as seeds for the synthesis of SLF@SGF@SF core–shell NCs were obtained as described by the step 2.3.3, except that $Sr(TFA)_2$ (0.5 mmol) was added instead of $Gd(TFA)_3$ (0.5 mmol) and $Sr(TFA)_2$ (1 mmol) . The obtained NCs were redispersed in 5 mL of chloroform or dried at 70 °C.

2.3.5. Synthesis of Hydrophilic SLF@SGF@SF NCs. SLF@SGF@SF NCs (0.2 mL) were dropwised in DI water containing 0.3 g of PEI. The solution was heated to 40 °C for 24 h. The solution was cooled to RT naturally, and products were precipitated with ethanol, centrifuged, and washed with DI water and ethanol in sequence. Finally, the products were redispersed in DI water.

2.4. Trimodal Bioimaging. *2.4.1. Cell Culture and Cytotoxicity Assay.* A549 cells were cultured in 96 well plates at 3×10^3 per well in Dulbecco's modified Eagle's medium (DMEM) at 37 °C and 5% CO_2. After 4 h, the hydrophilic UCNPs with different doses (5, 10, 25, 50, 100, 200, and 500 $\mu g \cdot mL^{-1}$) were added into the cells. The cells were incubated for another 24 h, and then 20 μL of MTT solution (5 $mg \cdot mL^{-1}$) was added to per cell well. After 4 h of incubation, media were removed, and then 150 μL of DMSO was added. The optical density (OD) of the mixture was measured by microplate reader at 490 nm. The cell viability (%) was calculated as $(OD_{treated}/OD_{control}) \times 100\%$ ($OD_{control}$ and $OD_{treated}$, respectively, were obtained in the absence and presence of hydrophilic UCNPs.).

2.4.2. Up-Conversion Luminescence Bioimaging. A549 cells were cultured in 96 well plates at 3×10^3 per well in DMEM at 37 °C and 5% CO_2. After 24 h, the hydrophilic SLF@SGF@SF NCs (200 $\mu g \cdot mL^{-1}$) were added to the cells. Overnight at 37 °C, all cells were washed three times with phosphate buffer saline after the removal of media. Next, the cells were fixed for 15 min with cell fixatives and washed three times. The nuclei were counter-stained for 10 min with 0.1 $\mu g \cdot mL^{-1}$ DAPI staining solution and washed three times. Up-conversion optical bioimaging was performed under a confocal laser scanning microscope.

2.4.3. MR Imaging. SLF@SGF@SF NC aqueous solutions with varying concentration of Gd^{3+} (4.0, 2.0, 1.0, 0.5, 0.25, and 0.125 mM) were placed in a series of 1.5 mL tubes for in vitro T_1-weighted MRI. For in vivo MR imaging, 0.5 mL of SLF@SGF@SF NC aqueous solutions with 8 mM of Gd^{3+} was intravenously administrated into the mice. The T_1-weighted MR images were obtained by a 1.5 T human clinical scanner (Siemens Medical System).

2.4.4. CT Imaging. To evaluate the capability of CT imaging, the SLF@SGF@SF NCs at different concentrations (30, 15, 7.5, 3.75, 1.875, and 0.938 $mg \cdot mL^{-1}$) were dispersed in saline for in vitro CT imaging. For in vivo CT imaging, 0.5 mL of SLF@SGF@SF NC aqueous solutions (30 $mg \cdot mL^{-1}$) was intravenously administrated into the mice. CT images were acquired using JL M.U.A NO.2 HOSP Philips, iCT 256 Scanner (Philips Medical System).

2.4.5. Animal Administration. Mice (19–22 g) were anesthetized through intraperitoneal injection of 10 wt % chloral hydrate. Subsequently, the NCs were intravenously injected into the mice for both MR and CT imaging.

3. RESULTS AND DISCUSSION

3.1. Strcuture and Morphology of the NCs. The SLF (core-only), SLF@SGF (one layer of core–shell) and SLF@SGF@SF (two layers of core–shell) up-conversion NCs have been obtained by high-temperature decomposition and oriented epitaxial growth. Due to the XRD patterns of the reported Sr_2LuF_7 (tetragonal, JCPDS 82-0640), Sr_2GdF_7 (tetragonal, JCPDS 53-0775), and SrF_2 (cubic, JCPDS 06-0262) are very similar. The lattice between core and shell matched so well that the core–shell NCs are easy to form. The phase structures and crystallinities of the as-synthesized up-conversion NCs were investigated by XRD. As Figure 1 shows, the as-prepared NCs have good crystallinities, and their diffraction peak positions and intensities coincide well with the literature values.

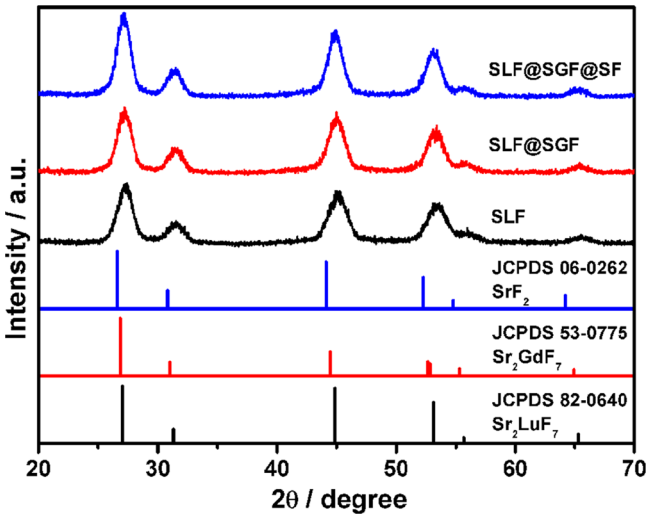

Figure 1. XRD patterns of SLF, SLF@SGF, and SLF@SGF@SF NCs.

The size and morphology of the up-conversion NCs were examined by TEM. Representative low-magnification transmission electron microscopy (TEM) images are shown in Figure 2a–c. As one can see, the average grain diameter of up-conversion NCs increases with the introduction of shell. The SLF and SLF@SGF samples are ball-like regular particles. However, the SLF@SGF@SF nanoparticles gradually become cubes as the particle size becomes larger. In Figure 2d–f, the corresponding high-magnification TEM images clearly demonstrate that the obtained monodisperse and homogeneous up-conversion NCs possess very small particle sizes. As statistically shown in Figure S1, the average grain diameters of SLF, SLF@SGF, and SLF@SGF@SF up-conversion NCs are 6.36, 7.29, and 8.27 nm, respectively. In the typical high-resolution TEM (HRTEM) images of these NCs (Figure 2g–i), the lattice fringes on the individual up-conversion NCs are very legible. The spacings of the lattice fringes are estimated about 0.332, 0.335, and 0.334 nm, which correspond to the (213) plane of Sr_2LuF_7, the (102) plane of Sr_2GdF_7, and the (111) plane of SrF_2, respectively. The corresponding fast Fourier transform (FFT) pattern of Figure 2i is shown in the inset of Figure 2f, which reveals that the core–shell NCs have a single crystalline feature. Meanwhile, the EDX spectral analysis (Figure S2) of

DOI: 10.1021/acsami.6b14007
ACS Appl. Mater. Interfaces 2017, 9, 5748–5756

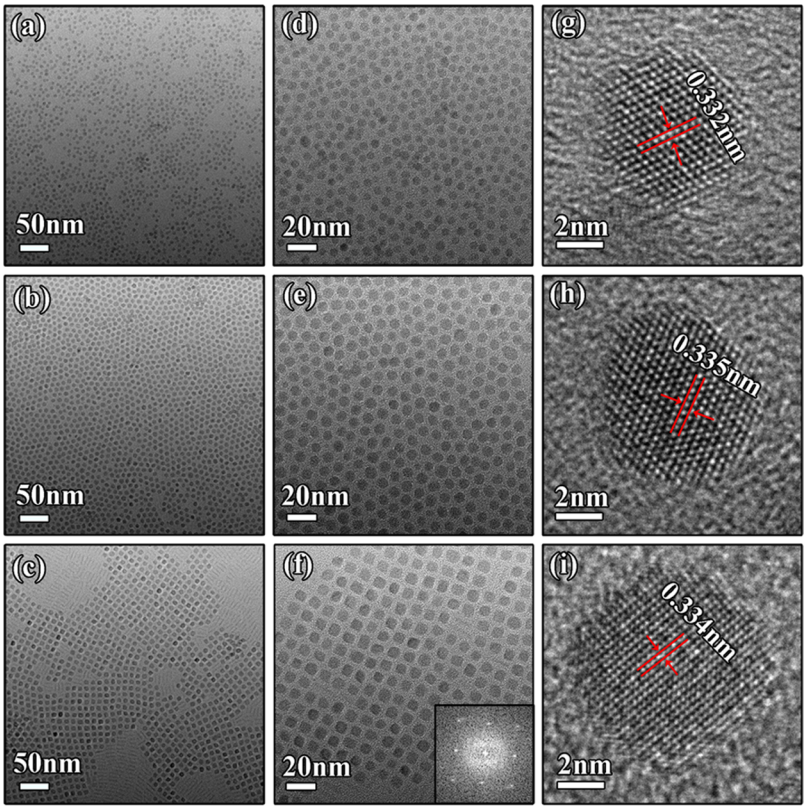

Figure 2. TEM images of SLF, SLF@SGF, and SLF@SGF@SF NCs. Representative TEM images (a–c), high-magnification TEM images (d–f), HRTEM images (g–i), and the corresponding FFT patterns of panel i (panel f inset).

SLF@SGF confirms the presence of Sr, F, Lu, Gd, Yb, and Er elements. Moreover, we can adjust the thickness of the outer shell by controlling the addition amount of shell precursor. With the increase of the amount of precursor of the outer shell, the particle size of the obtained core–shell up-conversion NCs becomes larger, as shown in Figure S3. These results demonstrate that we can control the synthesis of this kind of core–shell up-conversion NCs.

3.2. Up-Conversion Luminescent Properties. For lanthanide-doped nanomaterials, their luminescence properties are very important. The low luminescence efficiency of up-conversion nanomaterials has been troubling scientific researchers. As is known, core–shell structure can effectively reduce the surface defects and harmful nonradiative transition to increase the up-conversion luminescence efficiency. We take Sr_2LuF_7 as the host matrix, Yb^{3+} as the sensitizer, and Er^{3+} as the emitter to obtain the core-only up-conversion NCs. It is important to note that the concentration of Yb^{3+} and Er^{3+} must be controlled at a low concentration because the high concentration of doping can cause the concentration luminescence quenching. Therefore, we chose a common doping ratio (Sr_2LuF_7:18%Yb/2%Er). In terms of the up-conversion luminescence process, the sensitizer Yb^{3+} absorbed the excitation of 980 nm, followed by energy transfer to the emitter Er^{3+} that emits visible light. As Figure 3 shows, the up-conversion luminescence of Sr_2LuF_7:18%Yb/2%Er NCs is not strong. To enhance the up-conversion luminescence intensity, an inert homogeneous shell Sr_2GdF_7 was coated on the surface of SLF to obtain SLF@SGF. It is easy to observe that the up-conversion luminescence intensity has been significantly improved, which is about 10 times of that of core-only. Due to long-term toxicity of rare earth ions reported by some

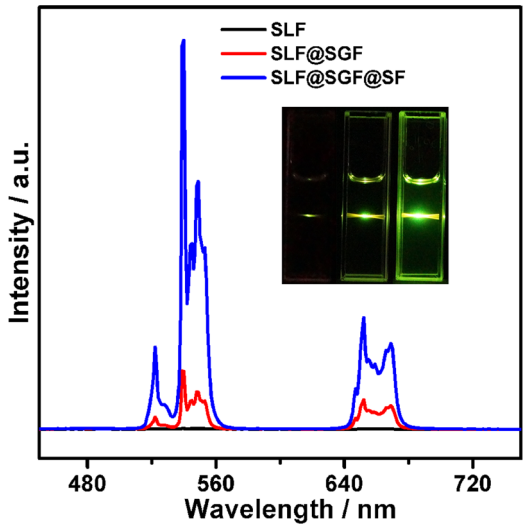

Figure 3. Up-conversion luminescence emission spectra of SLF, SLF@SGF, and SLF@SGF@SF in cyclohexane. Insets are the corresponding fluorescence photographs.

papers, we selected SrF_2 as the outer shell coating on the surface of SLF@SGF. On the one hand, the outer shell SrF_2 can increase the biocompatibility; on the other hand, the up-conversion luminescence efficiency of the whole core–shell NCs can also be improved. The up-conversion luminescence emission spectra and corresponding luminescence photographs (Figure 3 and insets) clearly demonstrate the change of up-conversion luminescence intensity from SLF and SLF@SGF to SLF@SGF@SF NCs. A total of three characteristic peaks at

DOI: 10.1021/acsami.6b14007
ACS Appl. Mater. Interfaces 2017, 9, 5748–5756

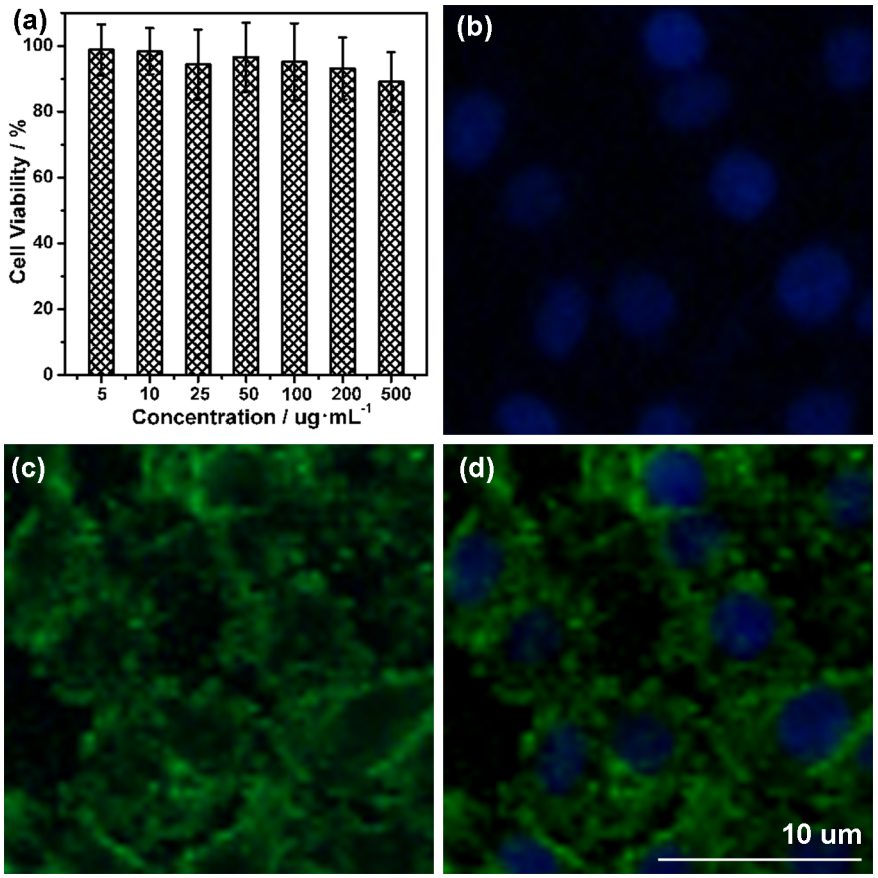

Figure 4. (a) Cell viability of A549 cells incubated with SLF@SGF@SF NCs for 24 h, (b–d) confocal microscopy images of A549 cells. Blue and green colors respectively represented up-conversion luminescence emissions and DAPI-stained cell nucleus.

525, 545, and 650 nm were recorded, which can be ascribed to the transitions of $^4H_{11/2}$, $^4S_{3/2}$, and $^4F_{9/2}$ to $^4I_{15/2}$ of Er, respectively.

3.3. Trimodal Bioimaging. For bioapplication, it is required that the NCs must be dispersed in water. The as-prepared core–shell SLF@SGF@SF up-conversion NCs obtained from oil-phase medium cannot be directly used for bioimaging. Therefore, we transferred the SLF@SGF@SF NCs from hydrophobic to hydrophilic using a ligand-exchange method reported before.[43] Figure S4 is the representative TEM image of hydrophilic core–shell SLF@SGF@SF up-conversion NCs coated by PEI, which demonstrates that the size and shape of NCs were substantially unchanged and the monodispersity had a little change but did not affect further bioapplication. Meanwhile, the up-conversion luminescence emission spectra of hydrophobic and hydrophilic core–shell SLF@SGF@SF NCs were recorded, as shown in Figure S5. The up-conversion luminescence emission of hydrophilic NCs is weaker than that of hydrophobic ones due to the interaction between water molecules and NCs, but it can still meet the needs of up-conversion luminescence bioimaging.

Although the excellent optical properties and water solubility demonstrated that the as-prepared NCs have great potential in bioapplications, cytotoxicity is still a key consideration. To further illustrate the low cytotoxicity of the as-prepared hydrophilic core–shell SLF@SGF@SF up-conversion NCs, MTT assay was performed. Figure 4a shows the viability of HeLa cells after culturing with varying concentrations of hydrophilic core–shell SLF@SGF@SF up-conversion NCs for 24 h. The viability of cells that were not treated was assumed to be 100%. Upon culturing with 5 $\mu g \cdot mL^{-1}$ after 24 h of exposure, less than 5% of the cells were dead. When the culturing concentration of hydrophilic core–shell up-conversion NCs was increased to 500 $\mu g \cdot mL^{-1}$, the viability of cells was still nearly 90%. All of these data indicate that the as-prepared hydrophilic core–shell SLF@SGF@SF up-conversion NCs have negligible cytotoxicity and good biocompatibility.

As stated earlier, the as-prepared core–shell up-conversion NCs have excellent optical property and great potential for up-conversion luminescent bioimaging. In this paper, we employed the core–shell NCs as up-conversion luminescence probes for cell bioimaging. Figure 4b–d shows the in vitro bioimaging of A549 cells incubated with these core–shell NCs for 12 h at 37 °C and 5% CO_2 recorded by a confocal laser scanning microscope. The blue emission in Figure 4b came from cell nucleus stained by DAPI. The green image of cells (Figure 4c) was the up-conversion luminescence signal at 540 nm. Figure 4d shows the overlap of panels b and c in Figure 4, which illustrates that the as-prepared core–shell upcoversion NCs are mainly located in the cells. Therefore, these core–shell up-conversion NCs without background interference have great potential in cell bioimaging.

Apart from the excellent up-conversion luminescence, the core–shell up-conversion NCs are of magnetism because of the presence of Gd^{3+} ions in the middle shell. The magnetization curves of the SLF@SGF@SF NCs are shown in Figure 5a. As one can see, these NCs possess typical paramagnetism at room temperature, which is mainly ascribed to the unpaired electrons

DOI: 10.1021/acsami.6b14007
ACS Appl. Mater. Interfaces 2017, 9, 5748–5756

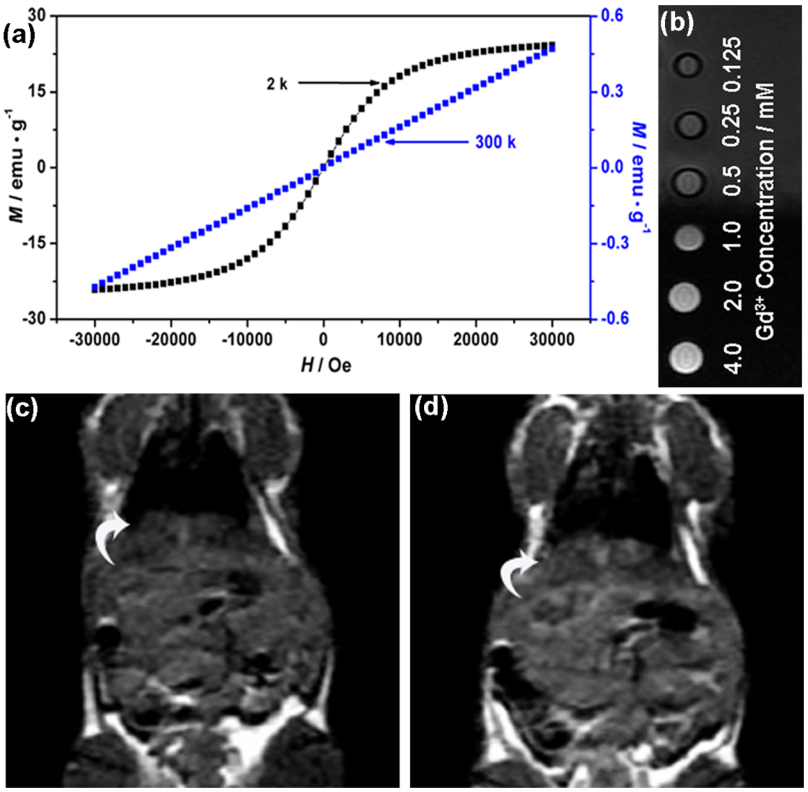

Figure 5. (a) Magnetization curves of SLF@SGF@SF NCs. (b) MR images of aqueous solutions of SLF@SGF@SF NCs with different Gd^{3+} concentration. In vivo MR coronal view images of a mouse before and after intravenous administration of 0.5 mL of SLF@SGF@SF NC aqueous solutions with 8.0 mM of Gd^{3+}: (c) preinjection and (d) after 24 h of injection.

of Gd^{3+}. The magnetization and mass susceptibility of the SLF@SGF@SF NCs were determined to be 0.48 emu·g^{-1} and 1.6 × 10^{-5} emu·Oe^{1-}·g^{-1}. MR imaging is a visual and noninvasive diagnostic method that is widely used in clinical medicine. The as-prepared NCs possess paramagnetism and the thickness of SrF_2 shell can be controlled. Therefore, to evaluate the potential of these core−shell SLF@SGF@SF NCs as T_1 MR imaging contrast agents, a proof-of-concept application was performed. Figure 5b shows the MR images of aqueous solutions of SLF@SGF@SF NCs with different Gd^{3+} concentration. It is obvious that the T_1-weighted MR imaging signal intensity was enhanced by increasing the concentration of SLF@SGF@SF NCs. In addition, the relaxation times of Gd^{3+} with different concentrations were measured. The slope of Figure S6 is the specific relaxivity, which is calculated to be 0.1515 mM^{-1} s^{-1}. For further MR bioimaging, the core−shell SLF@SGF@SF up-conversion NCs was intravenously administrated into a mouse. The in vivo MR view images of a liver of the mouse before and after intravenous administration for 24 h are shown in Figure 5c,d. The MR imaging signal in the liver of the mouse was significantly enhanced after administration of SLF@SGF@SF NCs by observing the contrasts of the figures. The results suggest that the core−shell SLF@SGF@SF NCs are promising as contrast agents for MR imaging.

Due to the high X-ray absorption coefficient of Lu, Gd, and doped Yb and Er ions, the core−shell SLF@SGF@SF up-conversion NCs should have great potential as promising nanoparticle-based CT contrast agents. To evaluate the CT contrast efficacy, X-ray CT images were acquired using SLF@SGF@SF up-conversion NCs in aqueous solution with different concentrations. As shown in the inset of Figure S6, the signal was enhanced as the concentration of the as-prepared NCs was increased. There was a linear relationship between the measured CT numbers, called Hounsfield units (HU), and concentrations of the as-prepared core−shell NCs (Figure S6). These results revealed that the as-prepared SLF@SGF@SF core−shell up-conversion NCs had great potential as CT imaging probes and prompted us to assess their feasibility as in vivo CT imaging probes. A solution of the as-prepared SLF@SGF@SF core−shell up-conversion NCs was intravenously administered to a mouse, and the distribution of the NCs was tracked by X-ray CT imaging. As shown in panel a of Figure 6, the density of heart and liver tissue was not enhanced (determined based on the images of preinjection samples). However, after intravenous administration of NCs for 24 h, the liver was obviously enhanced compared to images of preinjection samples. The enhanced density of liver and spleen was observed after intravenous administration of NCs for 24 h (Figure 6b). However, images of the kidney and heart showed no obvious difference between preinjection and postinjection, which indicated that the NCs could be mainly accumulated in liver and spleen after injection for 24 h. Panels c and d show the corresponding 3D imagings of in vivo CT images, which are more intuitive to reflect the enhancement of NCs. Moreover, the CT value of each organ in axial section was measured, which was shown in Figure S6. All of the results demonstrate that the as-prepared SLF@SGF@SF core−shell up-conversion NCs could be good contrast agents for in vivo CT imaging.

4. CONCLUSIONS

In summary, we designed and synthesized sub-10 nm Sr_2LuF_7:Yb/Er@Sr_2GdF_7@SrF_2 core−shell up-conversion

DOI: 10.1021/acsami.6b14007
ACS Appl. Mater. Interfaces 2017, 9, 5748−5756

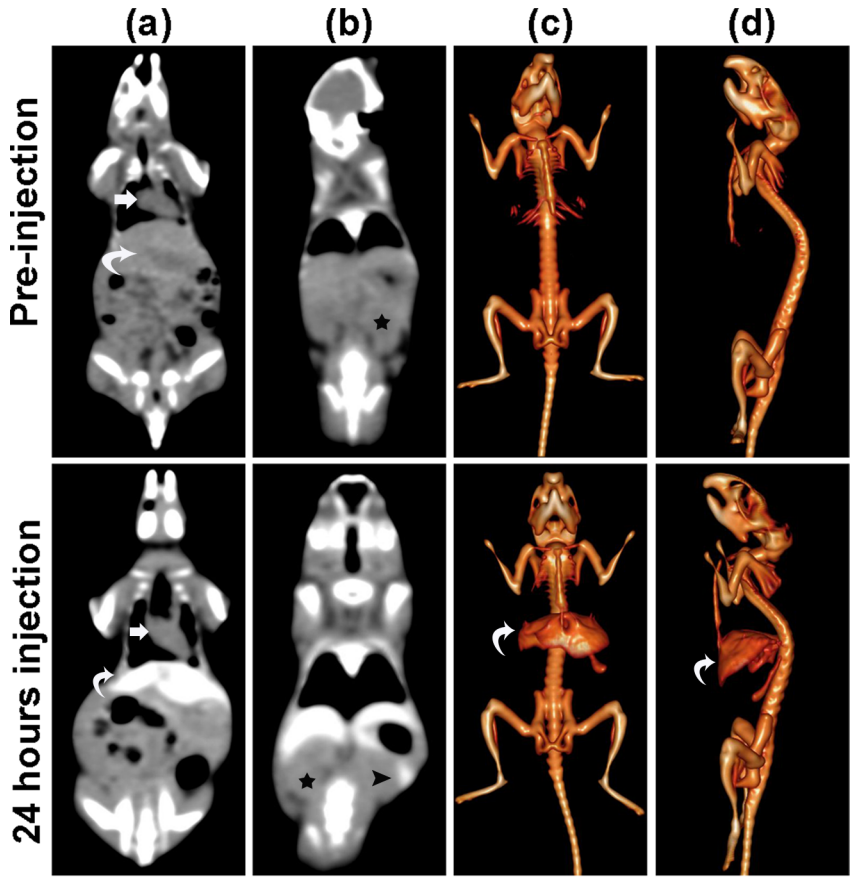

Figure 6. In vivo CT view images of a mouse before and after intravenous administration of 0.5 mL of SLF@SGF@SF NC aqueous solutions (30 mg·mL^{-1}): (a) heart (arrow) and liver (curved arrow), (b) spleen (arrowhead) and kidney (star), and (c and d) the corresponding 3D renderings of in vivo CT images.

NCs by a seed-mediated growth process for the first time. A great enhancement in up-conversion luminescence intensity was achieved because of the core−shell nanostructure. The MTT assay and up-conversion luminescence bioimaging demonstrate that these NCs have low biotoxcity and can act as promising up-conversion luminescence probes. In addition, the paramagnetic property of NCs and in vivo MR imaging reveal that the NCs have potential in MR imaging. Moreover, the NCs as promising CT contrast agents were investigated in detail in mice. All of these results indicate that the core−shell up-conversion NCs we designed can serve as promising contrast agent for up-conversion luminescence−MR−CT trimodal bioimaging.

■ ASSOCIATED CONTENT

Supporting Information

The Supporting Information is available free of charge on the ACS Publications website at DOI: 10.1021/acsami.6b14007.

A histogram of the particle size distribution, EDX spectra and TEM images of the core−shell up-conversion NCs, the emission spectra of hydrophobic and hydrophilic core−shell NCs, the relaxation rate for the different Gd^{3+} concentrations, CT values (HU) for the various concentrations of core−shell NCs, and the biodistribution after 24 h of injection compared to pre-injection conditions. (PDF)

■ AUTHOR INFORMATION

Corresponding Authors

*E-mail: zshi@mail.jlu.edu.cn.
*E-mail: cglee@jlu.edu.cn.

ORCID

Zhan Shi: 0000-0001-9717-1487

Author Contributions

C.C. and J.L. contributed equally to this work. All authors have contributed to the manuscript preparation and given approval to the final version of the manuscript.

Notes

The authors declare no competing financial interest.

■ ACKNOWLEDGMENTS

This work was supported by the Foundation of the Natural Science Foundation of China (grant nos. 21621001, 21371069, and 21301068) and the S&T Development Program of Jilin Province of China (grant no. 20160101325JC). This project was also supported by the State Key Laboratory of Luminescence and Applications (SKLA-2015-08).

■ REFERENCES

(1) Sun, M.; Xu, L.; Ma, W.; Wu, X.; Kuang, H.; Wang, L.; Xu, C. Hierarchical Plasmonic Nanorods and Upconversion Core-Satellite Nanoassemblies for Multimodal Imaging-Guided Combination Phototherapy. *Adv. Mater.* **2016**, *28*, 898−904.

(2) Zhang, L.; Zeng, L.; Pan, Y.; Luo, S.; Ren, W.; Gong, A.; Ma, X.; Liang, H.; Lu, G.; Wu, A. Inorganic Photosensitizer Coupled Gd-based

DOI: 10.1021/acsami.6b14007
ACS Appl. Mater. Interfaces 2017, 9, 5748−5756

Upconversion Luminescent Nanocomposites for in Vivo Magnetic Resonance Imaging and Near-infrared-responsive Photodynamic Therapy in Cancers. *Biomaterials* **2015**, *44*, 82−90.
(3) Chen, C.; Li, C.; Li, T.; Liu, J.; Huang, H.; Bai, T.; Wang, Z.; Shi, Z.; Feng, S. Water-Soluble, Monodisperse, Lanthanide-Doped Y(Gd)-VO_4 Nanocrystals as Promising Multimodal Bioprobe. *Eur. J. Inorg. Chem.* **2015**, *2015*, 3108−3115.
(4) Tian, Q.; Hu, J.; Zhu, Y.; Zou, R.; Chen, Z.; Yang, S.; Li, R.; Su, Q.; Han, Y.; Liu, X. Sub-10 nm Fe_3O_4@$Cu_{2-x}S$ Core-shell Nanoparticles for Dual-modal Imaging and Photothermal Therapy. *J. Am. Chem. Soc.* **2013**, *135*, 8571−8577.
(5) Liu, J.; Liu, Y.; Bu, W.; Bu, J.; Sun, Y.; Du, J.; Shi, J. Ultrasensitive Nanosensors Based on Upconversion Nanoparticles for Selective Hypoxia Imaging in Vivo upon Near-infrared Excitation. *J. Am. Chem. Soc.* **2014**, *136*, 9701−9709.
(6) Li, F.; Li, C.; Liu, X.; Chen, Y.; Bai, T.; Wang, L.; Shi, Z.; Feng, S. Hydrophilic, Upconverting, Multicolor, Lanthanide-doped $NaGdF_4$ Nanocrystals as Potential Multifunctional Bioprobes. *Chem. - Eur. J.* **2012**, *18*, 11641−11646.
(7) Liu, B.; Chen, Y.; Li, C.; He, F.; Hou, Z.; Huang, S.; Zhu, H.; Chen, X.; Lin, J. Poly(Acrylic Acid) Modification of Nd3+-Sensitized Upconversion Nanophosphors for Highly Efficient UCL Imaging and pH-Responsive Drug Delivery. *Adv. Funct. Mater.* **2015**, *25*, 4717−4729.
(8) Wang, Y. F.; Liu, G. Y.; Sun, L. D.; Xiao, J. W.; Zhou, J. C.; Yan, C. H. Nd^{3+}-sensitized Upconversion Nanophosphors: Efficient in vivo Bioimaging Probes with Minimized Heating Effect. *ACS Nano* **2013**, *7*, 7200−7206.
(9) Li, F.; Li, C.; Liu, J.; Liu, X.; Zhao, L.; Bai, T.; Yuan, Q.; Kong, X.; Han, Y.; Shi, Z.; Feng, S. Aqueous Phase Synthesis of Upconversion Nanocrystals through Layer-by-layer Epitaxial Growth for in Vivo X-ray Computed Tomography. *Nanoscale* **2013**, *5*, 6950−6959.
(10) Yang, D.; Dai, Y.; Liu, J.; Zhou, Y.; Chen, Y.; Li, C.; Ma, P.; Lin, J. Ultra-small $BaGdF_5$-based Upconversion Nanoparticles as Drug Carriers and Multimodal Imaging Probes. *Biomaterials* **2014**, *35*, 2011−2023.
(11) Tian, G.; Zheng, X.; Zhang, X.; Yin, W.; Yu, J.; Wang, D.; Zhang, Z.; Yang, X.; Gu, Z.; Zhao, Y. TPGS-stabilized $NaYbF_4$:Er Upconversion Nanoparticles for Dual-modal Fluorescent/CT Imaging and Anticancer Drug Delivery to Overcome Multi-drug Resistance. *Biomaterials* **2015**, *40*, 107−116.
(12) Zhang, H.; Wu, H.; Wang, J.; Yang, Y.; Wu, D.; Zhang, Y.; Zhang, Y.; Zhou, Z.; Yang, S. Graphene Oxide-$BaGdF_5$ Nanocomposites for Multi-modal Imaging and Photothermal Therapy. *Biomaterials* **2015**, *42*, 66−77.
(13) Yi, Z.; Lu, W.; Liu, H.; Zeng, S. High Quality Polyacrylic Acid Modified Multifunction Luminescent Nanorods for Tri-modality Bioimaging, in Vivo Long-lasting Tracking and Biodistribution. *Nanoscale* **2015**, *7*, 542−550.
(14) Liu, Q.; Chen, M.; Sun, Y.; Chen, G.; Yang, T.; Gao, Y.; Zhang, X.; Li, F. Multifunctional Rare-earth Self-assembled Nanosystem for Tri-modal Upconversion Luminescence/Fluorescence/Positron Emission Tomography Imaging. *Biomaterials* **2011**, *32*, 8243−8253.
(15) Wang, Y.; Song, S.; Liu, J.; Liu, D.; Zhang, H. ZnO-functionalized Upconverting Nanotheranostic Agent: Multi-modality Imaging-guided Chemotherapy with On-demand Drug Release Triggered by pH. *Angew. Chem.* **2015**, *127*, 546−550.
(16) Rieffel, J.; Chen, F.; Kim, J.; Chen, G.; Shao, W.; Shao, S.; Chitgupi, U.; Hernandez, R.; Graves, S. A.; Nickles, R. J.; Prasad, P. N.; Kim, C.; Cai, W.; Lovell, J. F. Hexamodal Imaging with Porphyrin-phospholipid-coated Upconversion Nanoparticles. *Adv. Mater.* **2015**, *27*, 1785−1790.
(17) Park, Y. I.; Lee, K. T.; Suh, Y. D.; Hyeon, T. Upconverting Nanoparticles: a Versatile Platform for Wide-field Two-photon Microscopy and Multi-modal in Vivo Imaging. *Chem. Soc. Rev.* **2015**, *44*, 1302−1317.
(18) Peng, J.; Xu, W.; Teoh, C. L.; Han, S.; Kim, B.; Samanta, A.; Er, J. C.; Wang, L.; Yuan, L.; Liu, X.; Chang, Y. T. High-efficiency in Vitro and in Vivo Detection of Zn^{2+} by Dye-assembled Upconversion Nanoparticles. *J. Am. Chem. Soc.* **2015**, *137*, 2336−2342.
(19) Wang, X.; Zhuang, J.; Peng, Q.; Li, Y. A General Strategy for Nanocrystal Synthesis. *Nature* **2005**, *437*, 121−124.
(20) Chen, C.; Li, C.; Shi, Z. Current Advances in Lanthanide-Doped Upconversion Nanostructures for Detection and Bioapplication. *Adv. Sci.* **2016**, *3*, 1600029.
(21) Boyer, J. C.; van Veggel, F. C. Absolute Quantum Yield Measurements of Colloidal $NaYF_4$:Er^{3+},Yb^{3+} Upconverting Nanoparticles. *Nanoscale* **2010**, *2*, 1417−1419.
(22) Zhou, D.; Liu, D.; Xu, W.; Yin, Z.; Chen, X.; Zhou, P.; Cui, S.; Chen, Z.; Song, H. Observation of Considerable Upconversion Enhancement Induced by $Cu_{2-x}S$ Plasmon Nanoparticles. *ACS Nano* **2016**, *10*, 5169−5179.
(23) Zhang, H.; Li, Y.; Ivanov, I. A.; Qu, Y.; Huang, Y.; Duan, X. Plasmonic Modulation of the Upconversion Fluorescence in $NaYF_4$:Yb/Tm Hexaplate Nanocrystals Using Gold Nanoparticles or Nanoshells. *Angew. Chem., Int. Ed.* **2010**, *49*, 2865−2868.
(24) Wang, J.; Deng, R.; MacDonald, M. A.; Chen, B.; Yuan, J.; Wang, F.; Chi, D.; Andy Hor, T. S.; Zhang, P.; Liu, G.; Han, Y.; Liu, X. Enhancing Multiphoton Upconversion through Energy Clustering at Sublattice Level. *Nat. Mater.* **2013**, *13*, 157−162.
(25) Dong, H.; Sun, L. D.; Wang, Y. F.; Ke, J.; Si, R.; Xiao, J. W.; Lyu, G. M.; Shi, S.; Yan, C. H. Efficient Tailoring of Upconversion Selectivity by Engineering Local Structure of Lanthanides in Na_xREF_{3+x} Nanocrystals. *J. Am. Chem. Soc.* **2015**, *137*, 6569−6576.
(26) Huang, P.; Zheng, W.; Zhou, S.; Tu, D.; Chen, Z.; Zhu, H.; Li, R.; Ma, E.; Huang, M.; Chen, X. Lanthanide-doped $LiLuF_4$ Upconversion Nanoprobes for the Detection of Disease Biomarkers. *Angew. Chem., Int. Ed.* **2014**, *53*, 1252−1257.
(27) Wang, F.; Wang, J.; Liu, X. Direct Evidence of a Surface Quenching Effect on Size-dependent Luminescence of Upconversion Nanoparticles. *Angew. Chem., Int. Ed.* **2010**, *49*, 7456−7460.
(28) Chen, X.; Peng, D.; Ju, Q.; Wang, F. Photon Upconversion in Core-shell Nanoparticles. *Chem. Soc. Rev.* **2015**, *44*, 1318−1330.
(29) Xu, Z.; Quintanilla, M.; Vetrone, F.; Govorov, A. O.; Chaker, M.; Ma, D. Harvesting Lost Photons: Plasmon and Upconversion Enhanced Broadband Photocatalytic Activity in Core@Shell Microspheres Based on Lanthanide-Doped $NaYF_4$, TiO_2, and Au. *Adv. Funct. Mater.* **2015**, *25*, 2950−2960.
(30) Lv, R. C.; Yang, P. P.; He, F.; Gai, S. L.; Yang, G. X.; Lin, J. Hollow Structured Y_2O_3:Yb/Er-Cu_xS Nanospheres with Controllable Size for Simultaneous Chemo/Photothermal Therapy and Bioimaging. *Chem. Mater.* **2015**, *27*, 483−496.
(31) Rinkel, T.; Nordmann, J.; Raj, A. N.; Haase, M. Ostwald-ripening and Particle Size Focussing of Sub-10 nm $NaYF_4$ Upconversion Nanocrystals. *Nanoscale* **2014**, *6*, 14523−14530.
(32) Zheng, W.; Zhou, S.; Chen, Z.; Hu, P.; Liu, Y.; Tu, D.; Zhu, H.; Li, R.; Huang, M.; Chen, X. Sub-10 nm Lanthanide-doped CaF_2 Nanoprobes for Time-resolved Luminescent Biodetection. *Angew. Chem., Int. Ed.* **2013**, *52*, 6671−6676.
(33) Rinkel, T.; Raj, A. N.; Dühnen, S.; Haase, M. Synthesis of 10 nm ß-$NaYF_4$:Yb,Er/$NaYF_4$ Core/Shell Upconversion Nanocrystals with 5 nm Particle Cores. *Angew. Chem., Int. Ed.* **2016**, *55*, 1164−1167.
(34) Wang, F.; Han, Y.; Lim, C. S.; Lu, Y.; Wang, J.; Xu, J.; Chen, H.; Zhang, C.; Hong, M.; Liu, X. Simultaneous Phase and Size Control of Upconversion Nanocrystals through Lanthanide Doping. *Nature* **2010**, *463*, 1061−1065.
(35) Damasco, J. A.; Chen, G.; Shao, W.; Agren, H.; Huang, H.; Song, W.; Lovell, J. F.; Prasad, P. N. Size-tunable and Monodisperse Tm^{3+}/Gd^{3+}-doped Hexagonal $NaYbF_4$ Nanoparticles with Engineered Efficient Near Infrared-to-near Infrared Upconversion for in Vivo Imaging. *ACS Appl. Mater. Interfaces* **2014**, *6*, 13884−13893.
(36) Zhang, F.; Wan, Y.; Yu, T.; Zhang, F.; Shi, Y.; Xie, S.; Li, Y.; Xu, L.; Tu, B.; Zhao, D. Uniform Nanostructured Arrays of Sodium Rare-earth Fluorides for Highly Efficient Multicolor Upconversion Luminescence. *Angew. Chem., Int. Ed.* **2007**, *46*, 7976−7979.
(37) Liu, D.; Xu, X.; Du, Y.; Qin, X.; Zhang, Y.; Ma, C.; Wen, S.; Ren, W.; Goldys, E. M.; Piper, J. A.; Dou, S.; Liu, X.; Jin, D. Three-

DOI: 10.1021/acsami.6b14007
ACS Appl. Mater. Interfaces 2017, 9, 5748−5756

dimensional Controlled Growth of Monodisperse Sub-50 nm Heterogeneous Nanocrystals. *Nat. Commun.* **2016**, *7*, 10254.
(38) Yang, Y.; Tu, D.; Zheng, W.; Liu, Y.; Huang, P.; Ma, E.; Li, R.; Chen, X. Lanthanide-doped Sr_2YF_7 Nanoparticles: Controlled Synthesis, Optical Spectroscopy and Biodetection. *Nanoscale* **2014**, *6*, 11098−11105.
(39) Xia, Z.; Du, P.; Liao, L. Facile Hydrothermal Synthesis and Upconversion Luminescence of Tetragonal Sr_2LnF_7:Yb^{3+}/Er^{3+} (Ln = Y, Gd) Nanocrystals. *Phys. Status Solidi A* **2013**, *210*, 1734−1737.
(40) Ding, Y. F.; Li, R. W.; Nakai, M.; Majumdar, T.; Zhang, D. H.; Niinomi, M.; Birbilis, N.; Smith, P. N.; Chen, X. B. Osteoanabolic Implant Materials for Orthopedic Treatment. *Adv. Healthcare Mater.* **2016**, *5*, 1740−1752.
(41) Saidak, Z.; Marie, P. J. Strontium Signaling: Molecular Mechanisms and Therapeutic Implications in Osteoporosis. *Pharmacol. Ther.* **2012**, *136*, 216−226.
(42) Huang, Y.; Xiao, Q.; Hu, H.; Zhang, K.; Feng, Y.; Li, F.; Wang, J.; Ding, X.; Jiang, J.; Li, Y.; Shi, L.; Lin, H. 915 nm Light-Triggered Photodynamic Therapy and MR/CT Dual-Modal Imaging of Tumor Based on the Nonstoichiometric $Na_{0.52}YbF_{3.52}$:Er Upconversion Nanoprobes. *Small* **2016**, *12*, 4200−4210.
(43) Dai, Y.; Xiao, H.; Liu, J.; Yuan, Q.; Ma, P.; Yang, D.; Li, C.; Cheng, Z.; Hou, Z.; Yang, P.; Lin, J. In Vivo Multimodality Imaging and Cancer Therapy by Near-infrared Light-triggered Trans-platinum Pro-drug-conjugated Upconverison Nanoparticles. *J. Am. Chem. Soc.* **2013**, *135*, 18920−18929.

DOI: 10.1021/acsami.6b14007
ACS Appl. Mater. Interfaces 2017, 9, 5748−5756